Hindawi
Journal of Electrical and Computer Engineering
Volume 2023, Article ID 9813765, 1 page
https://doi.org/10.1155/2023/9813765

Retraction

Retracted: Seismic Performance Analysis of Fabricated Concrete Beam-Column Joints Based on Intelligent Finite Element Analysis

Journal of Electrical and Computer Engineering

Received 19 December 2023; Accepted 19 December 2023; Published 20 December 2023

This article has been retracted by Hindawi following an investigation undertaken by the publisher [1]. This investigation has uncovered evidence of one or more of the following indicators of systematic manipulation of the publication process:

(1) Discrepancies in scope

(2) Discrepancies in the description of the research reported

(3) Discrepancies between the availability of data and the research described

(4) Inappropriate citations

(5) Incoherent, meaningless and/or irrelevant content included in the article

(6) Manipulated or compromised peer review

The presence of these indicators undermines our confidence in the integrity of the article's content and we cannot, therefore, vouch for its reliability. Please note that this notice is intended solely to alert readers that the content of this article is unreliable. We have not investigated whether authors were aware of or involved in the systematic manipulation of the publication process.

Wiley and Hindawi regrets that the usual quality checks did not identify these issues before publication and have since put additional measures in place to safeguard research integrity.

We wish to credit our own Research Integrity and Research Publishing teams and anonymous and named external researchers and research integrity experts for contributing to this investigation.

The corresponding author, as the representative of all authors, has been given the opportunity to register their agreement or disagreement to this retraction. We have kept a record of any response received.

References

[1] C. Yang and X. Li, "Seismic Performance Analysis of Fabricated Concrete Beam-Column Joints Based on Intelligent Finite Element Analysis," *Journal of Electrical and Computer Engineering*, vol. 2022, Article ID 3659479, 11 pages, 2022.

Hindawi
Journal of Electrical and Computer Engineering
Volume 2022, Article ID 3659479, 11 pages
https://doi.org/10.1155/2022/3659479

Research Article

Seismic Performance Analysis of Fabricated Concrete Beam-Column Joints Based on Intelligent Finite Element Analysis

Chen Yang and Xiancheng Li

College of Civil Engineering and Architecture, Xinjiang University, Urumqi 830017, China

Correspondence should be addressed to Chen Yang; yangchen@stu.xju.edu.cn

Received 28 March 2022; Accepted 29 April 2022; Published 24 May 2022

Academic Editor: Wei Liu

In order to improve the seismic performance analysis effect of prefabricated concrete beam-column joints, this article uses intelligent finite element analysis technology to analyze the seismic performance of prefabricated concrete beam-column joints. Moreover, this article conducts in-depth research on the shear bearing capacity of the plastic hinge area so as to improve the accuracy of the calculation of the shear bearing capacity of the plastic hinge area. In addition, this article conducts finite element analysis of integral frame joints, uses finite element software to carry out numerical simulation of frame joints, and compares and analyzes the experimental results in the literature. Further, this article proposes an improvement of a prefabricated frame joint, performs finite element analysis on it, and compares and analyzes the numerical simulation results of concrete joints. The analysis results show that the finite element analysis model proposed in this article has high accuracy in the seismic performance analysis of prefabricated concrete beam-column joints, which meets the actual needs of the seismic performance analysis of modern prefabricated concrete beam-column joints.

1. Introduction

The prefabricated reinforced concrete structure is one of the important structural forms to realize building factories, and it is also the trend of building structure development. It breaks the traditional model and connects standardized prefabricated components through reliable connections. The use of prefabricated concrete components can reduce construction waste, maximize the utilization rate of building materials, meet the requirements of green development, and realize industrialized production methods [1]. The main weakness of the prefabricated reinforced concrete frame structure is the connection method of the components, and the connection of the nodes restricts the integrity and seismic performance of the structure. Wet connection and dry connection are the main connection methods for prefabricated concrete frames. The common connection methods of wet connection are grouting connection and postcast concrete, and the common connection methods of dry connection are bolt connection and welding [2]. With the continuous development of structural forms, the prefabricated shear wall structure and prefabricated laminated plate structure have become a structural system that changed the traditional model [3]. In order to improve the stability and integrity of prefabricated structures used in seismic areas, the research and application of joints are currently hot issues at home and abroad. The main purpose is to improve the mechanical performance, integrity, and overall seismic performance of the connection parts and ensure that the entire structure should have sufficient bearing capacity, strength, stiffness, energy dissipation, ductility, and the ability to resist dynamic loads such as earthquakes and wind. At the same time, the different ways of connecting nodes are also a factor that restricts the safety of prefabricated concrete beam-column member nodes.

In view of the problems existing in the traditional construction mode, the country has vigorously promoted the industrialization of construction in recent years, and the prefabricated concrete structure is one of the methods of industrialized construction. According to the existing

research, the precast concrete postcast monolithic joint is the mainstream hotspot of current application and research. However, postcast integral joints often have the problem of beam-column reinforcement bars colliding with each other. In order to avoid this problem, it is often necessary to take additional measures to ensure that the steel bars are accurately staggered from each other or directly change the cross-sectional size of the component and the arrangement position of the steel bar, which increases the difficulty of component prefabrication and increases the production cost. The hardness of ordinary steel bars is relatively large. If the on-site assembly operation cannot be carried out smoothly due to manufacturing errors, it will cause the assembly quality and speed. These factors also indirectly affect the advantages of prefabricated frame structures in engineering applications and become the bottleneck of large-scale promotion. The development of the industry is inseparable from the innovation of advanced technology. At present, my country's construction industrialization is still in its infancy, and there are still great deficiencies in the understanding, performance analysis, and design application of prefabricated concrete structure systems. The application of the prefabricated concrete system is mainly to copy the core production technology imported from abroad. However, the existing structural systems in foreign countries may not be able to adapt to my country's national conditions: most countries in Europe and Singapore are non-seismic areas and have low requirements for structural seismic performance; Japan's high-rise prefabricated concrete frame structure system adopts energy-consuming support technology to solve the problem and the seismic requirements are met, but the construction cost is high. It is an inevitable choice to promote the development of prefabricated concrete structures in my country to develop a prefabricated structural system that meets the economic and technical conditions of our country and meets the requirements of structural performance and strengthens technological innovation.

This article uses intelligent finite element analysis technology to analyze the seismic performance of prefabricated concrete beam-column joints to improve the application effect of prefabricated concrete members.

2. Related Work

At present, the research on concrete structures can be divided into two categories: structural test and numerical simulation. Structural testing is a traditional method of studying concrete structures [4]. The principle is simple, and it is easy to obtain the results intuitively. However, there are also disadvantages such as high test cost, long production cycle, and high test conditions [5]. Numerical simulation is a method of solving approximate solutions of mathematical models through computer program simulation, among which the finite element simulation method based on finite element theory is more commonly used [6]. With the continuous progress of science and technology, the finite element theory has also been further developed, making the finite element simulation method gradually become a new method of concrete structure research. The finite element method has sufficient accuracy in simulating the response of concrete structures under various working conditions and has no requirements for conditions such as test sites and concrete curing, which can greatly save research costs and is an important means of concrete research [7].

Literature [8] conducted low-cycle repeated loading tests on the edge and middle nodes of prestressed concrete beam columns to determine their hysteretic performance and shear resistance under earthquake action. The results show that the prestressed prefabricated concrete structure can greatly reduce the shear force of the beams and columns at the joints; when the displacement angle reaches 3%, both types of joints are only slightly damaged; the hysteretic energy dissipation capacity of the prestressed prefabricated concrete structure, although weaker, is still larger than expected, with negligible residual deformation and good seismic performance. Loading tests were carried out on a 3/5 scale 5-story prestressed prefabricated concrete frame structure to simulate its response to an earthquake. The frame structure is composed of 4 frames and 1 shear wall, in which the frame adopts prestressed hybrid connection, pretensioned prestressed connection, and two ordinary steel bar connections, a total of four different connection methods [9]. Under the simulated seismic load, in the direction of the shear wall, the structural damage is very small, only the concrete protective layer peels off at the bottom of the wall, and there are few cracks in the wall body; in the direction of the frame, the internal stress of the frame using the prestressed connection is far. When the displacement is less than the same displacement, the damage to the concrete is very small, and only slight cracks appear at the beam end [10]; although the maximum displacement angle between stories reaches 4.5%, which is twice the design value, the overall result is still impressive. Satisfactorily, the prestressed prefabricated concrete frame structure has good seismic performance, and this structural form can also be used in high-intensity areas. A form of prestressed prefabricated concrete hybrid connection joint is proposed, and 10 prestressed prefabricated concrete hybrid connection nodes are subjected to low-cycle repeated loading tests. The influence of the arrangement position of stress bars, the number of energy-dissipating bars, and the bonding conditions on the seismic performance of joints should be considered [11]. Compared with the concrete cast-in-place joint, the joint using the hybrid connection has the same energy dissipation capacity and strength, and the residual deformation is smaller [12]. In the unbonded prestressed prefabricated concrete structure, there is no bond between the prestressed tendons and the concrete, so it is more easily affected by the shear force. A low-cycle repeated loading test was carried out to study the shear resistance of the nodes. The results show that shear failure occurs in both types of joints; due to the poor bonding between the grouting mortar and the adjacent concrete in the bonded joints, the stress distribution of the prestressed tendons in the joints is different from that in the unbonded joints. Similar to [13], since there is no grouting mortar in the prestressed rib channel of the unbonded form node, the unbonded form node volume is smaller than the

bonded form, resulting in a volume difference; due to the existence of the volume difference, when the maximum interlayer shear force is reached, the strength degradation and shear deformation of the unbonded joints are larger than those of the bonded specimens [14]; the existence of volume difference leads to the shear bearing capacity of the unbonded joints being 10% smaller than that of the bonded joints; the degradation of shear resistance has a greater impact.

An experimental study was carried out on a prestressed fabricated concrete structure with additional dampers. The results show that the damper can improve the poor energy dissipation capacity of the prestressed prefabricated concrete structure, and the combination of the two provides great flexibility for the design [15]. The composite gradient steel strand can replace the prestressed tendons to apply prestress to each component, play the role of connecting each component, and can also play the role of energy dissipation element. Low-cycle repeated loading tests were carried out on the prestressed prefabricated concrete frame structures using gradient composite steel strands, unbonded prestressed tendons, and bonded prestressed tendons, and the stress characteristics of each form of frame structure were compared [16]. Compared with the structure using unbonded prestressed tendons, the structure using gradient composite steel strands can dissipate more energy; when the displacement angle reaches 2%, all three structures have no obvious damage [17]; the structure of composite steel strand is a more economical recoverable functional structure [18].

3. Intelligent Finite Element Analysis Algorithm

At present, the ductile seismic design concept in each code is realized through the deformation, absorption, and energy consumption of plastic dumplings, and different codes have different settings for plastic ammonium. The following is a brief introduction to the content of plasticity in each specification.

The formula for calculating the length of the equivalent plastic ammonium and the equivalent plastic ammonium length is as follows:

$$L_p = \min\begin{cases} 0 \cdot 08H + 0 \cdot 22 f_y d_x \geq 0 \cdot 044 f_y d_x, \\ \dfrac{2}{3} b. \end{cases} \tag{1}$$

In the formula, L_p is the equivalent plastic ammonium length, H is the height of the cantilever pier, and b is the section size. At the same time, f_y is the standard value of the tensile strength of the longitudinal reinforcement, and d_x is the size of the longitudinal reinforcement.

In addition, the code stipulates the minimum reinforcement ratio $\rho_{x,\min}$ of the densified stirrups in the potential plastic dumpling areas of circular and rectangular sections in areas with a fortification intensity of 7 and 8, respectively. It is calculated according to the following formula:

Circular section:

$$\rho_{x,\min} = \left[0 \cdot 14\eta_k + 5 \cdot 84\left(\eta_k - 1\right) + 0 \cdot 028\right] \frac{f_c'}{f_{yh}} \geq 0 \cdot 004. \tag{2}$$

Rectangular section:

$$\rho_{x,\min} = \left[0 \cdot 1\eta_k + 4 \cdot 17\left(\eta_k - 0 \cdot 1\right)\left(\rho_t - 0 \cdot 01\right) + 0 \cdot 02\right] \frac{f_c'}{f_{yh}} \geq 0.004. \tag{3}$$

In the formula, η_k is the axial compression ratio, ρ_t is the longitudinal reinforcement ratio, and f_c' is the peak stress of the restrained concrete. f_{yh} is the standard value of the tensile strength of stirrups.

The nominal axial force calculation of the plastic dumpling length is introduced, and the nominal axial force is defined as follows:

$$\eta_k = \frac{N_{Ed}}{A_c f_{ck}}. \tag{4}$$

In the formula, $N_{E\,d}$ is the design seismic axial load, Ac is the gross cross-sectional area of the concrete section, and f_{ck} is the concrete compressive strength.

(1) When there is $\eta_k \leq 0 \cdot 3$, the plasticity and length take the larger value of the following conditions:

(i) Section width in bending direction

(ii) The distance from the maximum bending moment to 80% of the maximum bending moment

When there is $0.3 \leq \eta_k \leq 0.6$, the design plastic ammonium length is 1.5 times that of the first case.

For the calculation of the equivalent plastic dumpling length, any value in the following formula is taken:

$$\begin{cases} L_p = 0 \cdot 08L_2 + 0 \cdot 022 f_{yd} d_s, \\ L_p = (0 \cdot 4 \sim 0 \cdot 6)H. \end{cases} \tag{5}$$

In the formula, H is the height of the section along the seismic action direction, L_2 is the length of the cantilever column, and f_{ye} is the yield strength of the longitudinal reinforcement. d_s is the diameter of the longitudinal r_{ib}.

The spacing s_L of the stirrups or transverse ties of the rectangular section shall meet the following conditions:

(1) There is $S_L \leq 6d_s$.

(2) $S_L \leq 6d_s$.

The minimum dimension of the core concrete to the center of the stirrups is $b_{\min}$, the lateral spacing of the stirrups or transverse tie bars is S_T, and $S_T \leq 1/3b_{\min}$.

For circular sections, the stirrup spacing S_L should meet the following conditions:

(1) There is $S_L \leq 6d_s$.

(2) $S_L \leq 1/5$, minimum dimension of core concrete to stirrup center.

(1) Bridge piers are divided into two types, as shown in Figure 1 below.

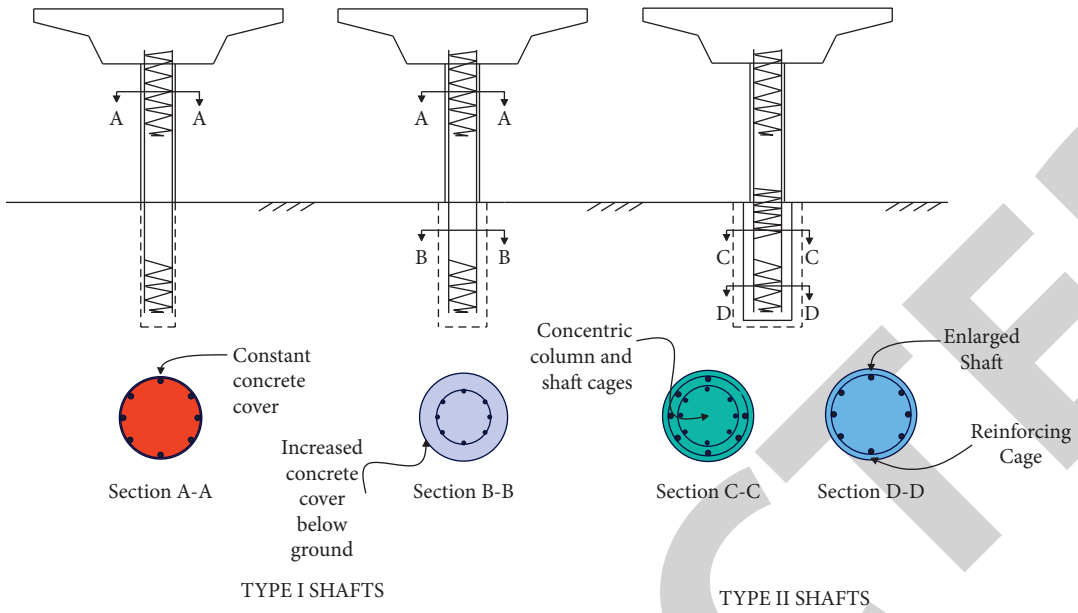

Figure 1: Main forms of bridge piers in the Caltrans specification in the United States.

(2) The potential plastic dumpling length takes the maximum value of the following conditions:

(1) 1.5 times the cross-sectional dimension of the bending direction;
(2) areas where the pier bending moment exceeds 75% of the maximum elastic bending moment;
(3) 0.25 times the distance from the maximum bending moment point to the reverse bending point.

(3) The calculation formula of the equivalent plastic dumpling length is as follows:

(1) For columns and piers of the second type,

$$L_p = \begin{cases} 0 \cdot 08L + 0 \cdot 15 f_{yd} d_{bl} \geq 0 \cdot 3 f_{ye} d_{bl} (in, ksi), \\ 0 \cdot 08L + 0 \cdot 022 f_{yd} d_{bl} \geq 0 \cdot 044 f_{ye} d_{bl} (mm, MPa). \end{cases} \tag{6}$$

(2) laterally isolated flared columns,

$$L_p = \begin{cases} G + 0 \cdot 3 f_{yd} d_{bl} (in, ksi), \\ G + 0 \cdot 044 f_{yd} d_{bl} (mm, MPa). \end{cases} \tag{7}$$

(i) In the formula, G is the distance between the independent taper hole and the bottom of the cover beam.

(3) The first type of pier:

$$L_p = D^* + 0 \cdot 08 H_{O-\max}. \tag{8}$$

(i) In the formula, D^* is the section size and $H_{O-\max}$ is the cantilever length.

(4) For the stipulations of the reinforced stirrups in the plastic ammonium area in the specification, the spacing of the stirrups shall be the minimum value of the following conditions:

(1) 0.2 times the minimum dimension of the cross-section of the column or half of the minimum dimension of the pier interface;
(2) 6 times the diameter of longitudinal steel bars;
(3) 220 mm.

The formula for calculating the length of plastic dumplings is as follows:

$$\begin{aligned} L_p &= 0 \cdot 2h - 0 \cdot 1D, \\ 0 \cdot 1D \leq L_p &\leq 0 \cdot 51D. \end{aligned} \tag{9}$$

In the formula, $V_{co} \leq \phi(0 \cdot 0023\sqrt{f_c'} A_e + V_s)$ is the length of the plastic ammonium zone, D is the width of the section, and h is the distance between the bottom of the pier and the action point of the superstructure.

It is stipulated in the detailed rules for seismic resistance of highway bridges that the calculation formula for the shear bearing capacity of the inclined section in the plastic ammonium zone is as follows:

$$V_{co} \leq \phi\left(0 \cdot 0023\sqrt{f_c'} A_e + V_s\right). \tag{10}$$

In the formula, V_{co} is the design value of shear force, f_c' is the standard compressive strength of concrete, and V_s is the shear resistance provided by stirrups. A_e is the effective shear area.

The formula for calculating the shear bearing capacity of the plastic dumpling area is as follows:

$$\begin{aligned} V &= 2 \cdot 5\tau_{Rd} A_e + f_{yv} \frac{0 \cdot 9\pi A_{sv}}{2s} D', \\ \tau_{R\,d} &= 0 \cdot 035 f_{ck}^{2/3}. \end{aligned} \tag{11}$$

In the formula, $\tau_{R\,d}$ is the shear strength of concrete, A_e is the effective shear area, and A_{sv} is the stirrup area.

Meanwhile, f_{yv} is the stirrup yield strength, and D' is the diameter of the stirrup ring.

The Caltrans code specifies that the shear capacity of the pier column is provided by concrete and stirrups; that is, $V_n = V_c + V_s$. The Caltrans code takes into account the influence of the ductility coefficient and the hoop ratio through factor 1, and the formula for calculating the shear bearing capacity of concrete is as follows:

$$V_c = v_c \times A_e. \tag{12}$$

In the plastic zone, there is

$$v_c = \text{factor } 1 \times \text{factor } 2 \times \sqrt{f_c'} \le 0 \cdot 33\sqrt{f_c'}. \tag{13}$$

Outside the plastic dumpling area, there is

$$v_c = 0 \cdot 25 \times \text{factor } 2 \times \sqrt{f_c'} \le 0 \cdot 33\sqrt{f_c'},$$

$$\text{factor } 1 = \frac{\beta_s, f_{yh}}{12 \cdot 5} + 0 \cdot 305 - 0 \cdot 083\mu_d \quad (0 \cdot 025 \le \text{factor } 1 \le 0 \cdot 25). \tag{14}$$

For the shear bearing capacity of stirrups, the principle of frame separation is usually used. ATC-32 adopts the 45° frame analysis model theory, and the calculation formula of the shear bearing capacity of stirrups is as follows:

There is a rectangular section:

$$V_s = \frac{A_v f_{yh} d}{s}, \tag{15}$$

There is a circular section:

$$V_s = \frac{\pi}{2} \frac{A_h f_{yh} D'}{s}. \tag{16}$$

In the above formula, f_{yh} is the yield strength of stirrups, and d is the spacing of stirrups in the calculation direction. D' is the diameter of the stirrup ring, and s is the stirrup spacing.

The shear capacity of the pier column is considered as two parts of the shear capacity of concrete and stirrups; that is,

$$\begin{aligned} P_s &= S_c + S_s, \\ S_c &= 10C_c C_s C_{pt} \tau_e bd, \\ S_s &= \frac{A_\omega \sigma_{sy} d(\sin\theta + \cos\theta)}{10 \times 1 \cdot 15a}. \end{aligned} \tag{17}$$

In the formula, P_s is the shear capacity of the pier column, S_e is the shear capacity of the concrete, and s_s is the shear capacity of the stirrup. Meanwhile, C_e is the earthquake type coefficient, C_s is the effective height correction coefficient of the section, and C_{pt} is the longitudinal reinforcement ratio coefficient. τ_e is the shear stress of concrete, b is the section width of the pier column, and A_ω is the area of the stirrup. Meanwhile, σ_{sy} is the stirrup yield strength, θ is the angle between the stirrup and the main axis, and a is the stirrup spacing.

When the ductile seismic design of the structure is carried out, we must first clarify the quantitative index of the ductile design. The following is a brief introduction to the ductility quantitative indicators in various specifications at home and abroad.

The curvature ductility coefficient and the displacement ductility ratio are often used to characterize the structural ductility. The nonlinear displacement ductility ratio is used in the specification of fabricated concrete joints, and the check calculation should meet the requirements of the following formula:

$$\mu_\mu = \frac{\Delta_{\max}}{\Delta_y} < [\mu_\mu]. \tag{18}$$

In the formula, μ_μ is the nonlinear displacement ductility ratio, $[\mu_\mu]$ is the allowable displacement ductility ratio, and $\Delta_{\max}$ is the nonlinear response maximum displacement of the bridge pier. Δ_y is the yield displacement of the pier.

The highway code does not propose a clear quantitative index of ductility design. In ductility design, only structural measures are taken for piers and joints, and corresponding ductility checks are not required.

The displacement ductility ratio u is used to characterize the structural ductility, and the calculation formula of the displacement ductility ratio is as follows:

$$\mu_d = \begin{cases} q, & T > T_0, \\ (q-1)\dfrac{T_0}{T} + 1 \le 5q - 4, & T < T_0, \end{cases} \tag{19}$$

$$T_0 = 1 \cdot 25T_c.$$

In the formula, T_c is the characteristic period of the response spectrum, and q is the behavior coefficient.

The index to characterize the structural ductility in the specification is the local displacement ductility ratio. The specific calculation formula is as follows:

(1) For cantilever piers, there is

$$\mu_c = \frac{\Delta_c}{\Delta_Y^{\text{col}}}. \tag{20}$$

(2) For bridge piers consolidated at both ends, there is

$$\begin{aligned} \mu_{c1} &= \frac{\Delta_{c1}}{\Delta_{Y1}^{\text{col}}}, \\ \mu_{c2} &= \frac{\Delta_{c2}}{\Delta_{Y2}^{\text{col}}}. \end{aligned} \tag{21}$$

The calculation of each parameter in the formula is as follows:

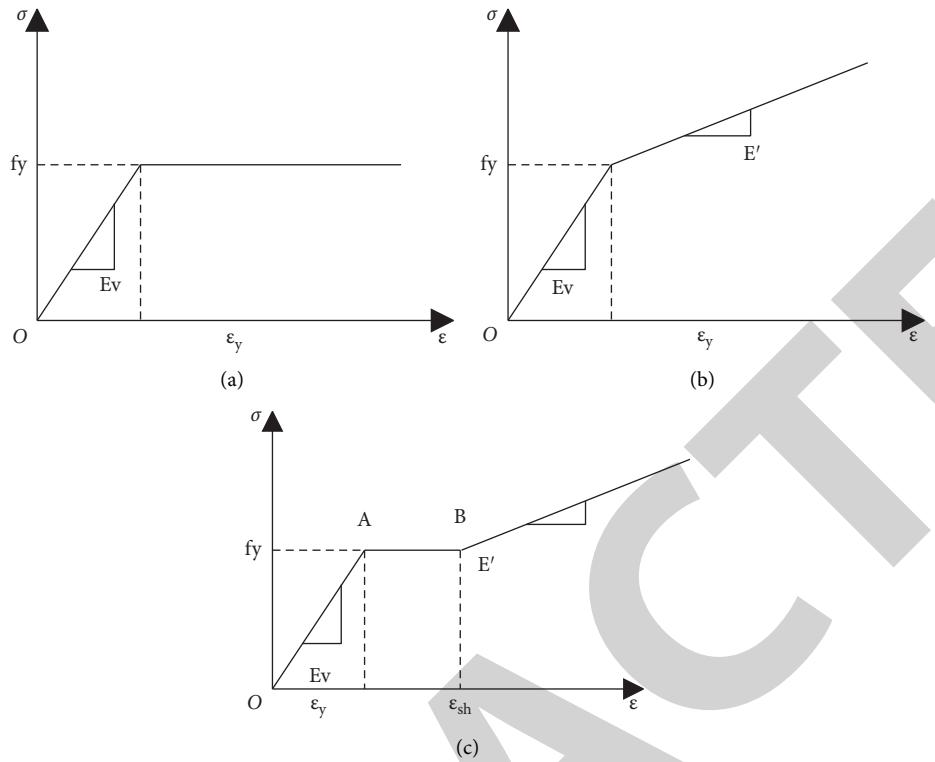

Figure 2: Reinforcing constitutive model. (a) Double straight line model. (b) Linear reinforced plasticity model. (c) Trilinear model.

$$
\begin{aligned}
&\Delta_c = \Delta_Y^{\mathrm{col}} + \Delta_p,\\
&\Delta_Y^{\mathrm{col}} = \frac{L^2}{3} \times \phi_Y,\\
&\Delta_p = \theta_p \times \left(\frac{L - L_P}{2}\right),\\
&\theta_p = L_p \times \phi_p,\\
&\phi_p = \phi_u - \phi_Y,\\
&\Delta_{c1} = \Delta_{Y1}^{\mathrm{col}} + \Delta_p, \Delta_{c2} = \Delta_{Y2}^{\mathrm{col}} + \Delta_p,\\
&\Delta_{Y1}^{\mathrm{col}} = \frac{L_1^2}{3} \times \phi_{Y1},\\
&\Delta_{Y2}^{\mathrm{col}} = \frac{L_2^2}{3} \times \phi_{Y2},\\
&\Delta_{p1} = \theta_{p1} \times \left(L - \frac{L_{P1}}{2}\right),\\
&\Delta_{p2} = \theta_{p2} \times \left(L - \frac{L_{P2}}{2}\right),\\
&\theta_{p1} = L_{p1} \times \phi_{p1},\\
&\theta_{p2} = L_{p2} \times \phi_{p2},\\
&\phi_{p1} = \phi_{u1} - \phi_{Y1}, \phi_{p2} = \phi_{u2} - \phi_{Y2}.
\end{aligned}
\tag{22}
$$

In the formula, L is the length of the cantilever, L_p is the length of the equivalent plastic dumpling, and Δ_p is the ideal plastic displacement caused by the immobility of the plastic dumpling. Δ_Y^{col} is the yield displacement formed by plastic ammonium deformation, and Δ_Y^{col} is the ideal yield obtained from the bending moment-curvature curve of the section.

Curvature: ϕ_p is the ideal plastic curvature of the section, ϕ_u is the curvature at the limit state of failure, and θ_p is the plastic rotation angle.

4. Seismic Performance Analysis of Fabricated Concrete Beam-Column Joints Based on Intelligent Finite Element Analysis

For steel, it has strong stability, as shown in Figure 2; it is a simplified model of steel. Among them, a, *b*, and *C* represent the double-line model, the linear reinforcement elastic model, and the three-line model, respectively. The analysis found that the stress growth of the three groups of models was different after reaching the yield stress. After the model a reaches the yield stress, the degree of denaturation gradually increases. However, the load is indeed on a straight line, which means that the load has not changed. The stress of the B model increases proportionally with the load. In the *C* model, the load does not change at first, and then the stress increases gradually. When the critical value is reached, the stress increases with the increase of the load.

The finite element analysis process mainly includes three steps: preprocessing, calculation and postprocessing. In the preprocessing, the solid model is first established, and the load and boundary conditions are determined. Next, the

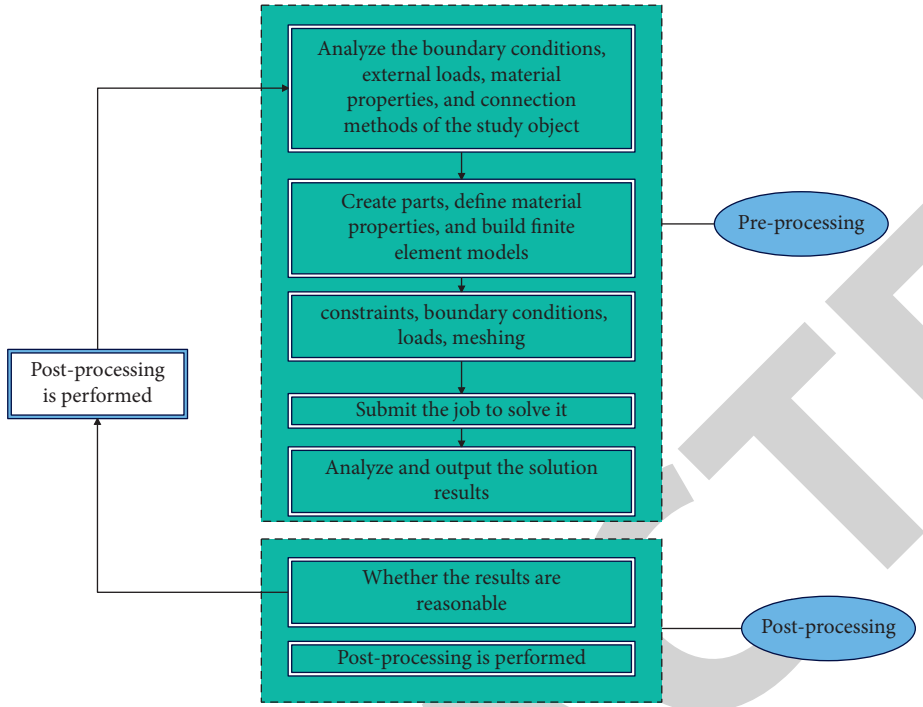

Figure 3: Steps of finite element analysis.

appropriate element type is selected. The solid model is discretized into multiple units, and the original continuum is represented by a set of units. Finally, loads and boundary conditions are applied. In the calculation process, the displacement distribution law is represented by the displacement function, and finally, the arbitrary displacement in the element is obtained by interpolation. Postprocessing is the display and analysis part of the calculation results, which can easily extract the stress and strain cloud diagrams under each load step and draw the hysteresis curve and skeleton curve of the entire loading process. The specific steps of finite element analysis are shown in Figure 3.

After the model is assembled, the constructed coordinate system is constrained by the top of the beam-column node. First, the model constrains the rotation and displacement of the X and Z axes. At this time, the Y-axis rotation angle is constrained, but care should be taken not to constrain its displacement. Subsequently, pressure was applied on the top of the column to ensure that the axial pressure ratio of the column was 0.4, which was basically the same as the experimental setting. At the bottom of the column, the three coordinate axes of the coordinate system are constrained by the rotation angle and displacement, and at the beam end, the rotation angle and displacement in the two directions of the X and Y axes are effectively constrained. At this time, it is necessary to pay attention to only constraining the corners in the Z direction and releasing their displacements. At the same time, it is also necessary to apply low-cycle repetitive loads from the beam ends. The loading value of the first cycle is taken as the concrete cracking load of 20 MPa, the loading value of the second cycle is taken as 70% of the experimental yield load, and the third cycle reaches yield. After yielding, the displacement-controlled loading is used, and the loading

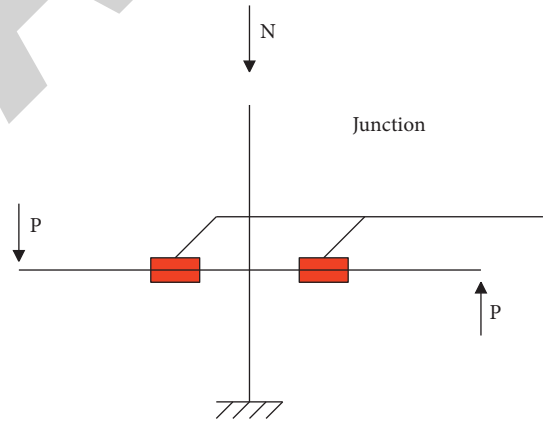

Figure 4: Loading regime.

was carried out according to the multiple of the yield displacement, and the cycle is repeated 3 times under each level of displacement until the load dropped to 85% of the peak load. Figure 4 shows a schematic diagram of specific node loading.

The process of using finite element software mainly includes building component modules, assigning material properties, assembling models, meshing models, relationships between modules, loads and constraints, submitting operations, and data extraction. ABAQUS/CAE consists of 10 functional modules, as shown in Figure 5. Among them, the modeling order on the left side of the figure is recommended by ABAQUS/CAE, but it is not static. After skilled software operation, the modeling order can be changed according to its own characteristics. Moreover, not all modules are used in modeling. For example, when analyzing

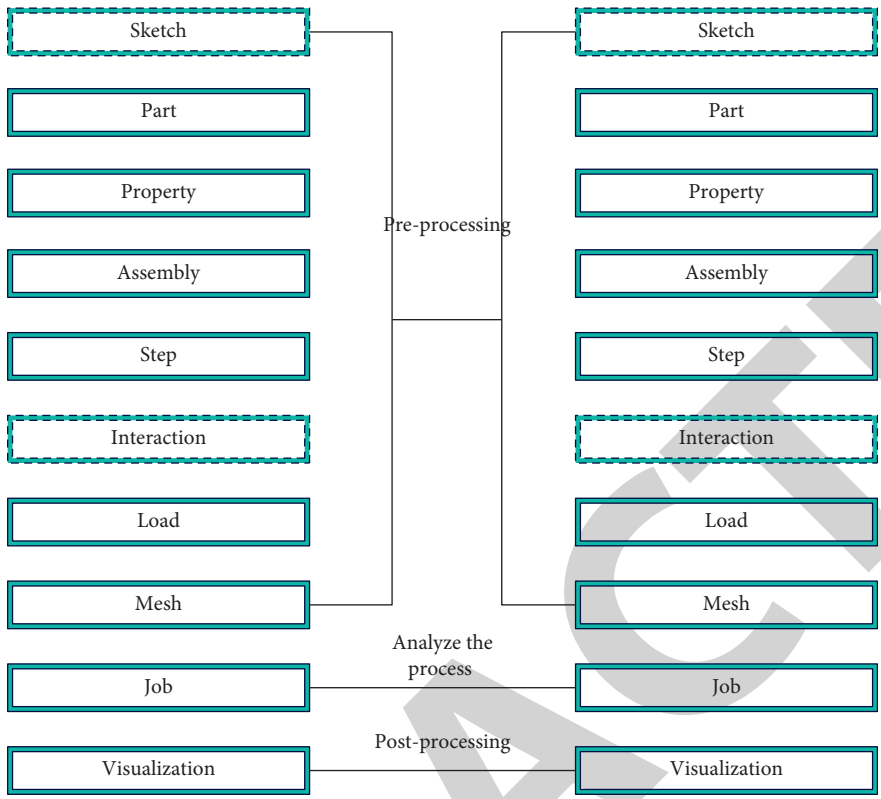

Figure 5: Finite element modeling process.

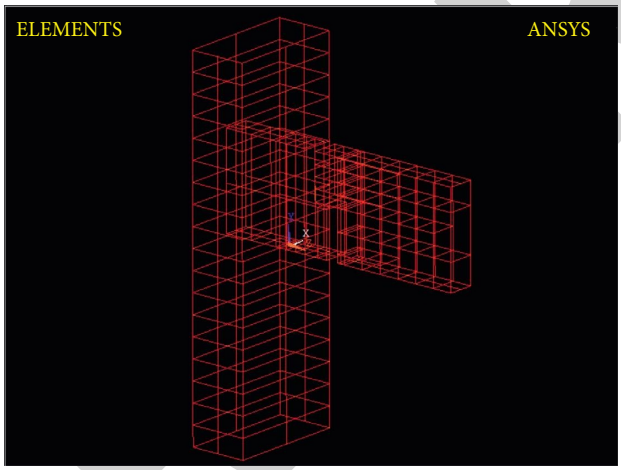

Figure 6: Reinforcing arrangement of beam-column joints.

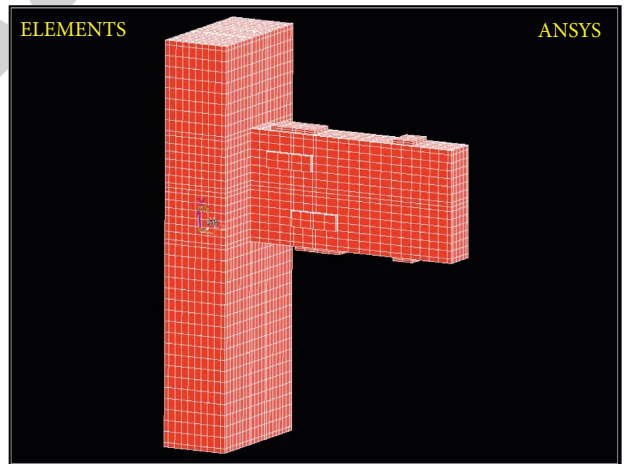

Figure 7: Finite element model of beam-column joint.

a single entity model, there is no need to define the interaction of Pan. Therefore, modeling should be determined according to its own needs.

The prefabricated concrete prestressed connection node is a node form that uses prestressed technology to realize the splicing of prefabricated components. According to the different methods of applying prestress, there are two forms of pretensioning and posttensioning methods. The advantages of prestressed connection assembly nodes are fast construction speed, short construction period, high labor production efficiency, and less on-site wet work. At the same time, due to the rebound effect of the prestressed tendons, the structure has a good self-recovery ability, and the residual deformation is small. However, the stress and deformation of reinforced concrete frame joints under the action of an earthquake are very complicated. With the rapid development of computer technology and the improvement of finite element theory, numerical simulation analysis plays an increasingly important role in the study of the seismic performance of frame joints.

On this basis, a case study is carried out. In this article, the reinforced finite element models of columns, beam corbels, and notched beams are established respectively, as shown in Figure 6. After the key points of the end stirrups

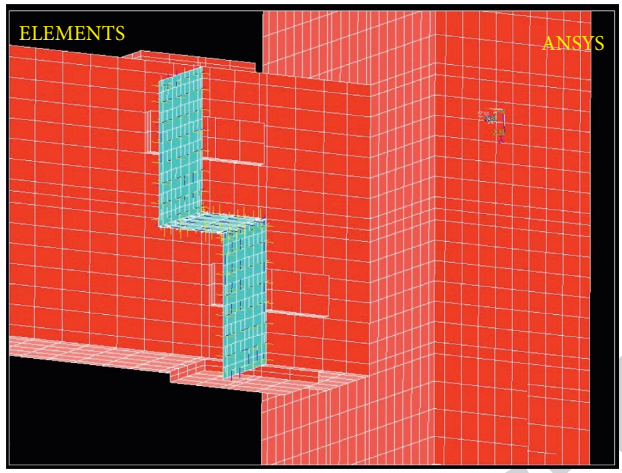

Figure 8: Contact elements in beam-column joint.

Table 1: Statistical table of the accuracy of system model simulation.

Num	Accuracy(%)	Num	Accuracy(%)	Num	Accuracy(%)	Num	Accuracy(%)
1	89.934	19	91.243	37	87.048	55	90.135
2	88.738	20	90.081	38	89.061	56	89.249
3	86.792	21	84.058	39	91.321	57	91.689
4	89.569	22	90.483	40	87.954	58	85.700
5	86.985	23	90.292	41	85.106	59	91.560
6	87.459	24	89.281	42	89.743	60	85.450
7	84.062	25	92.903	43	92.565	61	89.981
8	91.781	26	88.253	44	89.224	62	89.850
9	91.645	27	86.798	45	84.715	63	86.514
10	91.557	28	90.209	46	90.440	64	89.174
11	85.748	29	92.044	47	91.072	65	92.818
12	92.864	30	92.184	48	85.110	66	85.273
13	89.433	31	88.674	49	90.093	67	84.811
14	85.331	32	91.514	50	91.734	68	88.235
15	91.746	33	88.825	51	87.064	69	89.111
16	87.646	34	84.643	52	87.321	70	91.202
17	88.120	35	91.424	53	84.416	71	86.414
18	85.245	36	88.975	54	92.396	72	90.024

are created, the stirrups are established layer by layer through the loop statement command, and the key points of each corner point and the middle point are vertically connected into a line to form the longitudinal reinforcement. The real constant parameters are set to define the cross-section dimensions of the steel bars with different diameters and assign them to the corresponding steel bars. Finally, the element mesh is divided to establish the finite element model of the structural steel bars. A total of 1344 reinforcement elements are established for beam-column joints. Since the components of beam-column joints are relatively regular, the BLC5 command is used to sequentially create cuboid entities with the same dimensions as beams, columns and other components. Moreover, through the vglue command, the column, the full-section cuboid, and the half-section cuboid are bonded into a whole, and the geometric models of the column, the beam corbel, and the notched beam are established. Thirdly, the work plane is used to perform the cut-off operation along the x, y, and z directions at the connection, set the element mesh size, and perform the mapping mesh division, thereby forming the finite element model of the column, beam corbel, and notched beam. The total number of concrete elements to establish beam-column joints is 11945. The reinforcing arrangement of beam-column joints is shown in Figure 6. The constructed finite element model is shown in Figure 7.

The contact element is a highly nonlinear combination form based on the finite element model. In the finite element model of the fabricated beam-column joint, the contact between the beam corbel and the notched beam is surface-to-surface contact. There are three contact areas, namely, the side of the F part of the beam corbel and the side of the R part of the notched beam, the top surface of the R part of the beam corbel and the bottom surface of the R part of the notched beam, and the side of the R part of the beam corbel and the side of the F part of the notched beam. Because the concrete uses solid 65 three-dimensional solid elements, the contact element arrangement is shown in Figure 8.

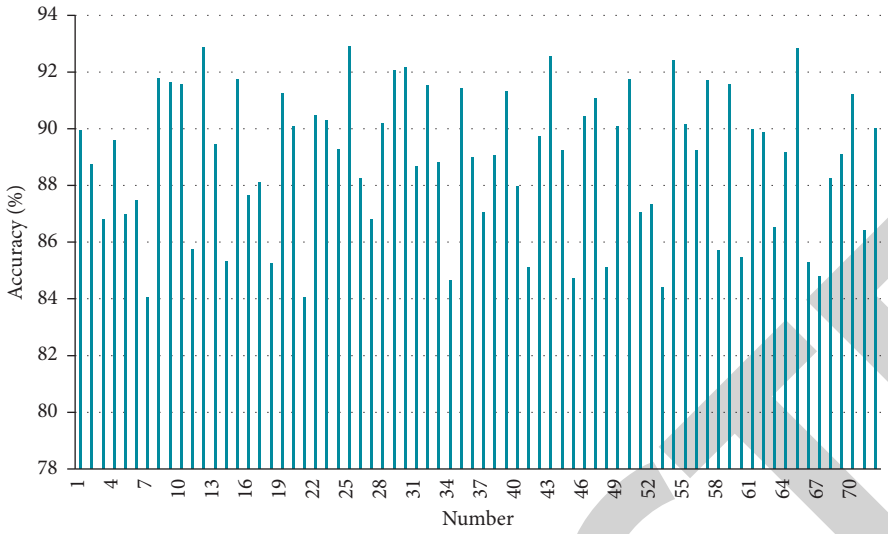

Figure 9: Statistical chart of the accuracy of model analysis.

After constructing the above model, the intelligent finite element analysis model of this article is used to analyze the seismic performance of prefabricated concrete beam-column joints, and the accuracy of the system model analysis in this article is calculated, and the results shown in Table 1 and Figure 9 are obtained.

From the above analysis, it can be seen that the finite element analysis model proposed in this article has high accuracy in the seismic performance analysis of prefabricated concrete beam-column joints, which meets the actual needs of the seismic performance analysis of modern prefabricated concrete beam-column joints.

5. Conclusion

The so-called prefabricated concrete structure means that the main components of the building are processed and manufactured in the factory and then transported to the site by means of transportation to assemble the components together in a reliable connection method. It reduces the number of workers required on-site and at the same time reduces on-site wet work and concrete maintenance work, which is conducive to realizing the green development requirements of "four sections and one environmental protection." At present, the research and application of prefabricated concrete structures in China mostly focus on prefabricated shear wall structures. In fact, the frame structure is easier to be modularized, standardized, and finalized, and the precast concrete frame structure has unique advantages in terms of promotion and application. This article uses intelligent finite element analysis technology to analyze the seismic performance of prefabricated concrete beam-column joints. The analysis results show that the finite element analysis model proposed in this article has a high accuracy rate in the seismic performance analysis of prefabricated concrete beam-column joints, which meets the actual needs of the seismic performance analysis of modern prefabricated concrete beam-column joints.

Data Availability

The labeled dataset used to support the findings of this study is available from the corresponding author upon request.

Conflicts of Interest

The authors declare that they have no conflicts of interest.

Acknowledgments

This study was sponsored by Xinjiang University.

References

[1] O. Guerra-Santin and S. Silvester, "Development of Dutch occupancy and heating profiles for building simulation," *Building Research & Information*, vol. 45, no. 4, pp. 396–413, 2017.

[2] T. Dodd, C. Yan, and I. Ivanov, "Simulation-based methods for model building and refinement in cryoelectron microscopy," *Journal of Chemical Information and Modeling*, vol. 60, no. 5, pp. 2470–2483, 2020.

[3] T. Abuimara, W. O'Brien, B. Gunay, and J. S. Carrizo, "Towards occupant-centric simulation-aided building design: a case study," *Building Research & Information*, vol. 47, no. 8, pp. 866–882, 2019.

[4] P. Remmen, M. Lauster, M. Mans, M. Fuchs, T. Osterhage, and D. Muller, "TEASER: an open tool for urban energy modelling of building stocks," *Journal of Building Performance Simulation*, vol. 11, no. 1, pp. 84–98, 2018.

[5] N. Endo, E. Shimoda, K. Goshome, T. Yamane, T. Nozu, and T. Maeda, "Simulation of design and operation of hydrogen energy utilization system for a zero emission building," *International Journal of Hydrogen Energy*, vol. 44, no. 14, pp. 7118–7124, 2019.

[6] I. Beausoleil-Morrison, "Learning the fundamentals of building performance simulation through an experiential teaching approach," *Journal of Building Performance Simulation*, vol. 12, no. 3, pp. 308–325, 2019.

[7] C. Xiong, J. Huang, and X. Lu, "Framework for city-scale building seismic resilience simulation and repair scheduling with labor constraints driven by time–history analysis," *Computer-Aided Civil and Infrastructure Engineering*, vol. 35, no. 4, pp. 322–341, 2020.

[8] A. D. Black, "Wor(l)d-Building: simulation and metaphor at the mars desert research station," *Journal of Linguistic Anthropology*, vol. 28, no. 2, pp. 137–155, 2018.

[9] K. Hanson, L. Hernandez, and J. A. Banaski Jr, "Building simulation exercise capacity in Latin America to manage public health emergencies," *Health Security*, vol. 16, no. S1, pp. S-98–S-102, 2018.

[10] E. K. Wati and N. Widiansyah, "Design of learning media: modeling & simulation of building thermal comfort optimization system in building physics course," *Jurnal Pendidikan IPA Indonesia*, vol. 9, no. 2, pp. 257–266, 2020.

[11] C. W. Lee and S. J. Cho, "The development of converting program from sealed geological model to gmsh, COMSOL for building simulation grid," *Journal of the Korean Earth Science Society*, vol. 38, no. 1, pp. 80–90, 2017.

[12] C. Miller, D. Thomas, J. Kämpf, and A. Schlueter, "Urban and building multiscale co-simulation: case study implementations on two university campuses," *Journal of Building Performance Simulation*, vol. 11, no. 3, pp. 309–321, 2018.

[13] X. Xie and Z. Gou, "Building performance simulation as an early intervention or late verification in architectural design: same performance outcome but different design solutions," *Journal of Green Building*, vol. 12, no. 1, pp. 45–61, 2017.

[14] A. I. Adilkhodjayev, I. M. Mahamataliev, and S. S. Shaumarov, "Theoretical aspects of structural and simulation modeling of the macrostructure of composite building materials," *Journal of Tashkent Institute of Railway Engineers*, vol. 14, no. 2, pp. 3–14, 2019.

[15] P. de Wilde, D. A. Coley, and I. Walker, "The building performance gap: are modellers literate?" *Building Service Engineering Research and Technology*, vol. 38, no. 6, pp. 757–759, 2017.

[16] J. S. Pei, B. Carboni, and W. Lacarbonara, "Mem-models as building blocks for simulation and identification of hysteretic systems," *Nonlinear Dynamics*, vol. 100, no. 2, pp. 973–998, 2020.

[17] A. Brunelli, F. de Silva, A. Piro et al., "Numerical simulation of the seismic response and soil–structure interaction for a monitored masonry school building damaged by the 2016 Central Italy earthquake," *Bulletin of Earthquake Engineering*, vol. 19, no. 2, pp. 1181–1211, 2021.

[18] P. Andrio, A. Hospital, J. Conejero et al., "BioExcel building blocks, a software library for interoperable biomolecular simulation workflows," *Scientific Data*, vol. 6, no. 1, pp. 169–178, 2019.